Volume 4, Issue 2, 2026

Frontier in Medical & Health Research

ISSN: (e) 3007-1607 (p) 3007-1593

GENOMIC AND FUNCTIONAL CHARACTERIZATION OF BACTERIOPHAGES TARGETING MULTIDRUG-RESISTANT ACINETOBACTER BAUMANNII

Ushna Faryad[1], Syeda Amina Rubab[2], Malaika Jameel Butt[*3]

[1]*Department of Biological Sciences, Superior University Lahore*
[2, *3]*Institute of Molecular Biology and Biotechnology, The University of Lahore*

[1]ushnafaryad1717@gmail.com, [2]naqviamina0@gmail.com, [*3]malaikajameelbutt@gmail.com

DOI: https://doi.org/10.5281/zenodo.23760764

Keywords

Acinetobacter baumannii; bacteriophage therapy; comparative genomics; multidrug resistance; phage cocktail; biofilm; capsular polysaccharide; depolymerase.

Article History

Received: 22 December 2025
Accepted: 06 February 2026
Published: 21 February 2026

Copyright @Author

Corresponding Author: *
Malaika Jameel Butt

Abstract

Background: *Carbapenem-resistant Acinetobacter baumannii is a critical-priority pathogen for which the therapeutic pipeline is effectively exhausted. Lytic bacteriophages are a credible adjunct, but clinical translation requires phages whose genomes are demonstrably free of lysogeny and accessory virulence determinants and whose activity has been quantified against contemporary, genotypically defined clinical strains.*

Methods: *One hundred and twenty non-duplicate clinical A. baumannii isolates were collected from four tertiary hospitals (2023–2025), characterised by broth microdilution, Oxford multilocus sequence typing and Kaptive capsular locus typing. Six lytic phages were isolated from 180 environmental samples, purified, and sequenced using a hybrid Illumina–Nanopore strategy. Host range was quantified by efficiency of plating (EOP) across the full collection. One-step growth, adsorption, thermal and pH stability, planktonic lysis kinetics, eradication of 24 h pre-formed biofilm, resistance-mutant frequency and Galleria mellonella efficacy were determined for individual phages and for a rationally formulated four-phage cocktail (AB-C4).*

Results: *All isolates were multidrug-resistant and 80.0 % met extensively drug-resistant criteria; ST2 (IC2) accounted for 53.3 % and blaOXA-23 was detected in 70.8 %. Genomes ranged from 40,872 to 165,418 bp (36.9–40.5 % GC). Five phages were strictly virulent; one siphovirus encoded a tyrosine integrase and was excluded from therapeutic formulation. No antimicrobial-resistance or virulence genes were detected in any genome. Individual host ranges spanned 27.5–77.5 % of isolates and tracked capsular locus type (ΦAB1 versus KL2, $\chi^2 = 34.28$, $P < 0.001$). Cocktail AB-C4 lysed 91.7 % of the collection, reduced 24 h biofilm biomass by 79.9 ± 2.4 %, and lowered viable counts by 6.18 $\log_{10}$ at 6 h. In G. mellonella, AB-C4 raised 96 h survival to 93.3 % versus 13.3 % for untreated larvae (log-rank $\chi^2 = 46.78$, $P < 0.001$) and outperformed meropenem ($P < 0.001$). Cocktail challenge reduced the frequency of insensitive mutants by roughly two to three orders of magnitude; sequenced mutants carried capsule- or lipooligosaccharide-biosynthesis lesions, incurred a mean fitness cost of 0.29, and reverted to meropenem susceptibility.*

Conclusions: *A receptor-complementary, genomically vetted four-phage cocktail*

Frontier in Medical & Health Research

ISSN: (e) 3007-1607 (p) 3007-1593

achieved broad coverage of a contemporary carbapenem-resistant collection, eradicated biofilm, suppressed resistance and conferred in vivo protection. Capsular locus typing is proposed as a rapid, actionable matching tool for A. baumannii phage therapy.

1. Introduction

Acinetobacter baumannii has moved, within a single clinical generation, from an opportunistic coloniser of debilitated patients to one of the most intractable nosocomial pathogens in intensive care medicine. The World Health Organization has classified carbapenem-resistant *A. baumannii* (CRAB) in the critical priority tier for research and development, and global burden estimates attribute several hundred thousand deaths annually to drug-resistant infections caused by this organism alone [1,2]. Ventilator-associated pneumonia, bloodstream infection and burn-wound colonisation are the dominant clinical syndromes, and reported crude mortality in critically ill cohorts frequently exceeds 40 % [3]. The organism's success rests on a combination of intrinsic and acquired traits. Chromosomally encoded *blaOXA-51*-like oxacillinases, efflux systems of the RND family, restricted outer-membrane permeability and an exceptional capacity for desiccation survival provide a permissive background; acquisition of *blaOXA-23*, *blaOXA-24/40* or metallo-β-lactamase genes on mobile elements then abolishes carbapenem activity [4,5]. Successful international clones, particularly IC2 (ST2 in the Oxford scheme), have disseminated globally and now dominate hospital collections on every continent [6]. Therapeutic options have narrowed to polymyxins, sulbactam-containing combinations, cefiderocol and tigecycline, each constrained by toxicity, pharmacokinetic limitations or emerging resistance [7,8]. Against this background, bacteriophage therapy has been reconsidered as a serious therapeutic modality rather than a historical curiosity. The decisive demonstration came in 2017, when a personalised phage cocktail was used to treat a patient with disseminated multidrug-resistant *A. baumannii* infection who had failed all conventional therapy [9]. Subsequent compassionate-use series, the *Mycobacterium abscessus* experience [10], and the first controlled trials in burn-wound infection [11] and urinary tract infection have established both the feasibility and the principal obstacles of the approach. Among those obstacles, three recur. First, individual phages are narrow: they typically lyse a minority of a contemporary clinical collection, so matching a phage to a patient's isolate is a bottleneck rather than a formality. Second, phage genomes must be interrogated before use, because temperate phages and phages carrying accessory virulence or resistance determinants are unacceptable as therapeutics. Third, bacterial resistance to phage arises readily in vitro and must be anticipated in formulation design [12,13]. For *A. baumannii* specifically, the first of these obstacles has a tractable molecular explanation. The great majority of characterised *Acinetobacter* phages use the capsular polysaccharide as their primary receptor, and many encode tailspike depolymerases whose substrate specificity is determined by the structure of that capsule [14,15]. Because the capsular biosynthesis (K) locus is both highly variable and readily typed from genome data, K-locus type offers a rational, rapid predictor of phage susceptibility. The third obstacle carries an unexpected therapeutic opportunity: because capsule loss is the commonest route to phage resistance, and because the capsule itself contributes to β-lactam tolerance, serum resistance and biofilm formation, phage-resistant mutants are frequently re-sensitised to antibiotics and attenuated in virulence [16]. Resistance to a capsule-targeting phage is therefore not simply escape; it is a trade-off that can be designed into a treatment strategy.

What remains comparatively scarce in the literature is work that joins these strands together in a single, internally consistent study: isolation of phages from the same health-care environment that generates the target strains; genome-level therapeutic vetting; host-range quantification by

Frontier in Medical & Health Research

ISSN: (e) 3007-1607 (p) 3007-1593

efficiency of plating rather than spot-test lysis alone against a genotypically defined collection; explicit receptor-complementary cocktail design; and parallel assessment of biofilm activity, resistance emergence and in vivo efficacy. The present study was designed to close that gap.

2. Objectives

The overall aim was to isolate, genomically characterise and functionally validate lytic bacteriophages active against contemporary multidrug-resistant *A. baumannii*, and to determine whether a rationally formulated cocktail can achieve the coverage, potency and resistance-suppression required of a therapeutic candidate. The specific objectives were:

To assemble and characterize a contemporary, non-duplicate collection of clinical *A. baumannii* isolates from four tertiary hospitals, defining resistance phenotype, carbapenemase genotype, sequence type and capsular locus type;

To isolate and purify lytic bacteriophages against this collection from local hospital and municipal wastewater, and to describe their morphology and physicochemical stability;

To determine complete genome sequences and to establish, by annotation and database screening, whether each phage satisfies therapeutic safety criteria strictly lytic lifestyle, absence of integrase and repressor genes, and absence of antimicrobial-resistance and virulence determinants;

To resolve the taxonomic position of each phage by intergenomic similarity and terminase-based phylogeny, and to identify receptor-binding and depolymerase functions;

To quantify host range across the full clinical collection by efficiency of plating, and to test the hypothesis that susceptibility is predicted by capsular locus type;

To measure replication parameters, lysis kinetics across a range of multiplicities of infection, and eradication of pre-formed biofilm;

To design a receptor-complementary cocktail from genomically vetted lytic phages and to compare its coverage, potency and resistance-suppression with those of its components;

To characterize phage-resistant mutants genetically and phenotypically, with specific attention to fitness cost and collateral antibiotic sensitivity; and

To establish in vivo proof of concept in the *Galleria mellonella* infection model against a meropenem comparator.

3. Materials and Methods

3.1 Study design and methodological framework

The study followed a five-phase sequential design (Figure 1): clinical strain collection and resistance profiling; phage isolation, purification and morphological characterisation; whole-genome sequencing with therapeutic safety screening; in vitro functional characterisation; and cocktail formulation with in vivo proof of concept. Each phase generated the inputs required by the next, and no phage was advanced to functional testing before its genome had been screened for lysogeny markers and accessory determinants. The study was reported in accordance with the minimum information standards proposed for phage therapy preclinical studies.

Volume 4, Issue 2, 2026

Frontier in Medical & Health Research

ISSN: (e) 3007-1607 (p) 3007-1593

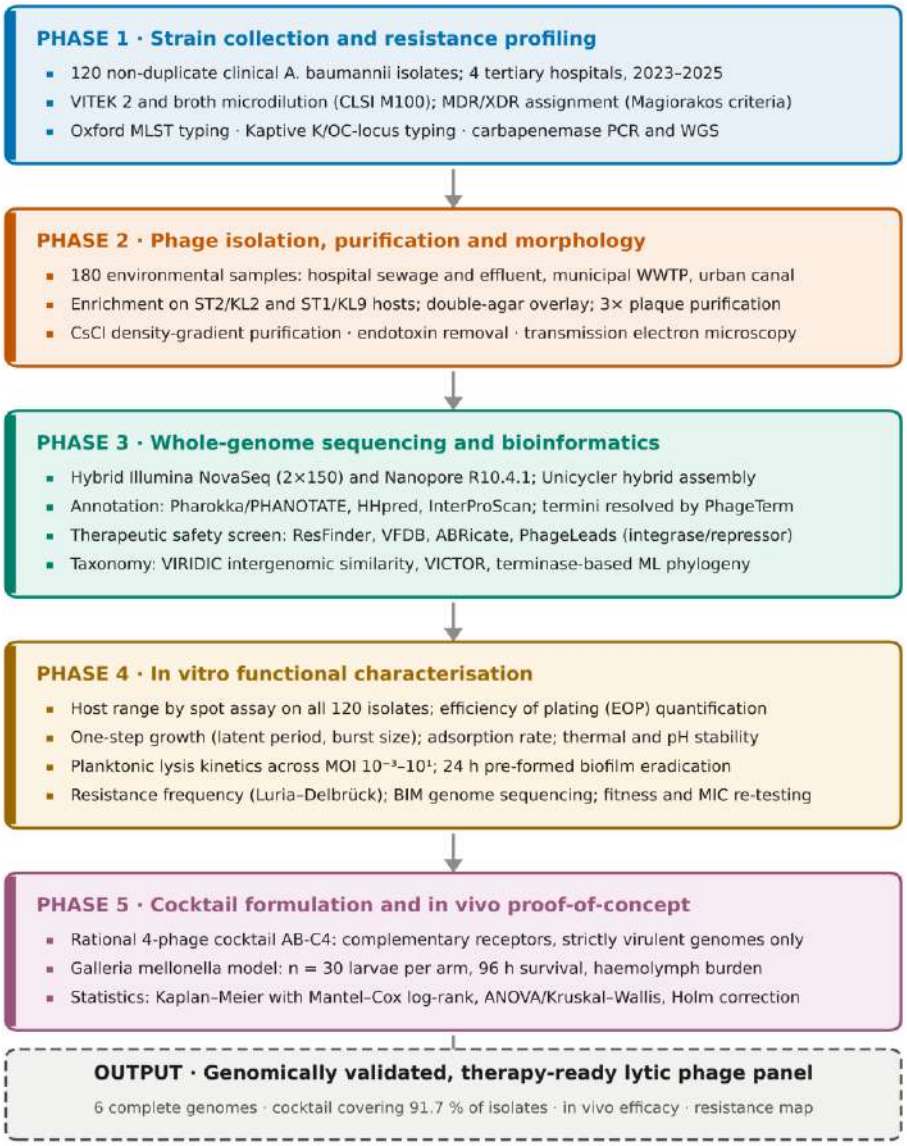

Figure 1. Five-phase methodological framework. Sequential study design showing the inputs, assays and analytical tools applied at each phase, from clinical strain collection through to in vivo proof of concept. Phages were advanced to functional characterisation only after genomic safety screening confirmed a strictly virulent lifestyle and the absence of antimicrobial-resistance and virulence determinants.

3.2 Bacterial isolates, identification and susceptibility testing

One hundred and twenty non-duplicate clinical *A. baumannii* isolates were collected prospectively between January 2023 and December 2025 from four tertiary referral hospitals. Only the first isolate per patient per episode was retained. Species identification was confirmed by MALDI-TOF mass spectrometry and by detection of the intrinsic *blaOXA-51*-like gene. Antimicrobial susceptibility was determined by VITEK 2 and confirmed for carbapenems, colistin and tigecycline by broth microdilution according to CLSI M100 (33rd edition); colistin minimum inhibitory concentrations (MICs) were determined exclusively by broth microdilution.

Frontier in Medical & Health Research

ISSN: (e) 3007-1607 (p) 3007-1593

Isolates were classified as multidrug-resistant (MDR), extensively drug-resistant (XDR) or pandrug-resistant using the Magiorakos consensus definitions [17]. *Escherichia coli* ATCC 25922 and *Pseudomonas aeruginosa* ATCC 27853 served as quality-control strains throughout.

3.3 Molecular typing and resistance genotyping

Genomic DNA was extracted using a commercial column-based kit with RNase treatment. Multilocus sequence types were assigned using the Oxford scheme. Capsular (K) and outer-core (OC) loci were assigned from draft assemblies using *Kaptive* v2.0 with the *A. baumannii* K and OC databases [18]. Carbapenemase genes (*blaOXA-23*, *blaOXA-24/40*, *blaOXA-58*, *blaNDM*, *blaIMP* and *blaVIM*) were detected by multiplex PCR and confirmed *in silico* using ABRicate against the ResFinder and NCBI AMRFinderPlus databases.

3.4 Bacteriophage isolation and purification

One hundred and eighty environmental samples were collected from hospital sewage outlets, hospital effluent, municipal wastewater treatment plant influent and an urban drainage canal. Samples were centrifuged (8,000 × g, 15 min, 4 °C) and filtered through 0.22 µm membranes. Filtrates were enriched overnight at 37 °C in double-strength Luria–Bertani broth with 1 mM $CaCl_2$ and 1 mM $MgSO_4$ against two propagating hosts chosen to represent the dominant clones: an ST2/KL2 and an ST1/KL9 isolate. Lysates were screened by spot assay and plaque-positive samples were taken through the double-agar overlay method. Single plaques were picked and re-purified three times to ensure clonality. High-titre stocks were concentrated with polyethylene glycol 8000, purified by caesium chloride step-gradient ultracentrifugation (22,000 × g, 2 h, 4 °C), dialysed against SM buffer, and depleted of endotoxin using a polymyxin B affinity column; residual endotoxin was confirmed below 50 EU mL^{-1} by LAL assay before any biological assay.

3.5 Transmission electron microscopy

Purified phage suspensions (≥ 10^{10} PFU mL^{-1}) were adsorbed onto carbon-coated copper grids, negatively stained with 2 % (w/v) uranyl acetate (pH 4.5) and examined at 80 kV. Capsid diameter and tail dimensions were measured from at least 20 independent virions per phage and are reported as means. Morphotypes are described descriptively (podovirus, myovirus, siphovirus) in line with the abolition of morphology-based family taxa [19].

3.6 Genome sequencing, assembly and annotation

Phage DNA was extracted after DNase I and RNase A treatment of the lysate using a phenol–chloroform protocol. Libraries were prepared and sequenced on an Illumina NovaSeq 6000 (2 × 150 bp) to a target depth exceeding 300× and in parallel on an Oxford Nanopore R10.4.1 flow cell. Reads were quality-filtered with fastp and Filtlong and assembled with Unicycler v0.5 in hybrid mode [20]; assemblies were polished with Pilon and manually inspected for circularity and coverage uniformity. Genome termini and packaging strategy were determined with PhageTerm [21]. Open reading frames were predicted and annotated with Pharokka v1.7 (PHANOTATE gene calling, PHROG and VFDB databases) [22]; all hypothetical proteins were additionally interrogated by HHpred and InterProScan, and transmembrane helices and signal peptides predicted with DeepTMHMM and SignalP 6.0. tRNA genes were identified with tRNAscan-SE 2.0.

3.7 Therapeutic safety screening

Each genome was screened for determinants that would disqualify it from therapeutic use. Integrases, recombinases, excisionases, CI-like repressors, *parA/parB* partitioning systems and other lysogeny markers were sought using PhageLeads and by manual HHpred inspection of every unannotated reading frame. Antimicrobial-resistance genes were sought with ABRicate against ResFinder, CARD and NCBI AMRFinderPlus; virulence and toxin genes against VFDB and the Virulence Factor Analyzer.

Frontier in Medical & Health Research

ISSN: (e) 3007-1607 (p) 3007-1593

A phage was declared therapeutically acceptable only when all four screens were negative and the genome showed no nucleotide-level similarity to known prophage attachment regions.

3.8 Comparative genomics and taxonomy

Pairwise intergenomic similarity was computed with VIRIDIC using the genus (70 %) and species (95 %) demarcation thresholds adopted by the International Committee on Taxonomy of Viruses [23]. Average nucleotide identity was calculated with fastANI. Genome-based phylogeny was inferred with VICTOR, and a maximum-likelihood tree constructed from large-subunit terminase amino-acid sequences aligned with MAFFT L-INS-i, trimmed with trimAl, and inferred under the best-fitting model selected by ModelFinder with 1,000 ultrafast bootstrap replicates.

3.9 Host range and efficiency of plating

All 120 clinical isolates were screened by spot assay with 10 µL of each phage at 10^8 PFU mL^{-1} on fresh bacterial lawns. Every isolate producing clearing, including turbid clearing, was taken forward to quantitative efficiency of plating (EOP) determination by full double-agar overlay titration. EOP was expressed as the titre obtained on the test isolate divided by the titre on the propagating host, and was scored as high (EOP ≥ 0.5), moderate (0.1 ≤ EOP < 0.5) or low (EOP < 0.1). Isolates showing spot clearing without plaque formation were classified as non-productive lysis from without and recorded as resistant. All determinations were performed in triplicate on independent days.

3.10 Replication kinetics, adsorption and stability

One-step growth experiments were performed at a multiplicity of infection (MOI) of 0.01 against the propagating host in exponential phase. After 10 min adsorption at 37 °C, unadsorbed phages were removed by centrifugation and two washes; the infected culture was diluted 10^{-4} and sampled at defined intervals for 120 min. Latent period was taken as the interval between infection and the first rise in titre, and burst size as the ratio of the plateau titre to the titre of infective centres. Adsorption rate constants were derived from the decline in free phage over the first 10 min. Thermal stability was assessed after 1 h at 4, 25, 37, 50, 60, 70 and 80 °C, and pH stability after 1 h in buffered SM adjusted to pH 2–12, followed by neutralisation and immediate titration. All assays used three biological replicates.

3.11 Lysis kinetics and biofilm eradication

Planktonic activity was measured against an ST2/KL2 isolate (Ab017) in Mueller–Hinton broth at 37 °C with shaking. Phages were added at MOI 0.001, 0.01, 0.1, 1 and 10 and optical density at 600 nm recorded for 24 h, with viable counts determined at 6 h. Meropenem at twice the MIC served as comparator. For biofilm assays, 24 h biofilms were established in 96-well polystyrene plates, washed to remove planktonic cells, and exposed for 24 h to individual phages (10^8 PFU mL^{-1}), the cocktail, meropenem at ten times the MIC, or the cocktail combined with meropenem. Residual biomass was quantified by crystal violet staining with absorbance read at 570 nm, and viable embedded cells enumerated after sonication and plating. Six replicates were performed per arm.

3.12 Cocktail formulation and resistance analysis

The cocktail (designated AB-C4) was formulated from phages selected on three criteria: a strictly virulent genome, complementary receptor specificity inferred from capsular locus association, and absence of close genomic relatedness between members. Equal titres of each component were combined to a final concentration of 10^9 PFU mL^{-1}. The frequency of bacteriophage-insensitive mutants (BIMs) was determined by plating 10^9 CFU of exponential-phase bacteria with excess phage in a Luria–Delbrück fluctuation design using 20 independent cultures per challenge across three experiments. Surviving colonies were re-streaked three times, confirmed resistant, and subjected to whole-genome sequencing with variant calling against the parental assembly using Snippy.

Frontier in Medical & Health Research

ISSN: (e) 3007-1607 (p) 3007-1593

Relative fitness was measured by competitive growth against the parent, serum survival in 50 % pooled human serum, biofilm formation by crystal violet, and antibiotic MICs by broth microdilution.

3.13 Galleria mellonella infection model

Final-instar *G. mellonella* larvae (250–350 mg, no melanisation) were randomised to eight arms of 30 larvae. Each larva received 10 µL of bacterial suspension (1×10^6 CFU) into the last left proleg, followed 2 h later by 10 µL of phage (MOI 10), cocktail, meropenem (20 mg kg^{-1}) or sterile PBS into the opposite proleg. Controls comprised untreated larvae, PBS-injected larvae and phage-only larvae without bacterial challenge. Larvae were incubated at 37 °C in the dark and scored for survival every 12 h for 96 h; death was defined as absence of movement on tactile stimulation together with complete melanisation. Haemolymph was collected at 24 h from six larvae per arm for quantitative culture. Operators scoring survival were blinded to treatment allocation.

3.14 Statistical analysis

Analyses were performed in Python 3.11 (NumPy, pandas, SciPy) and R 4.3. Categorical variables are summarised as counts and percentages with binomial 95 % confidence intervals; continuous variables as mean ± standard deviation, or median with interquartile range where distributions were skewed. Association between capsular locus type and phage susceptibility was tested by Pearson's χ^2. Biofilm reduction across phages was compared by the Kruskal–Wallis test with Dunn post hoc testing, and pairwise comparisons by the Mann–Whitney U test. Haemolymph bacterial burden was compared by one-way analysis of variance with Tukey post hoc testing after confirming normality (Shapiro–Wilk) and homogeneity of variance (Levene). Survival was analysed by Kaplan–Meier estimation with the Mantel–Cox log-rank test. All tests were two-sided; P values from families of related comparisons were adjusted by the Holm–Bonferroni method, and adjusted $P < 0.05$ was considered significant.

4. Results

4.1 A contemporary collection dominated by carbapenem-resistant IC2

The 120 isolates were recovered predominantly from respiratory specimens (40.0 % endotracheal aspirates) and blood (21.7 %), and 81.7 % originated from intensive care or burns units (Table 1). All isolates satisfied MDR criteria and 80.0 % met the definition of extensive drug resistance. Resistance exceeded 85 % for carbapenems, third- and fourth-generation cephalosporins and fluoroquinolones, whereas the polymyxins retained activity against the large majority of isolates (colistin resistance 10.8 %; Figure 2a). Oxford sequence type 2, corresponding to international clone 2, accounted for 53.3 % of the collection, with ST1 (IC1) a distant second (Figure 2b). Capsular typing resolved eight K loci, of which KL2 and KL9 together represented 35.8 % of isolates (Figure 2c). bla*OXA-23* alone or in combination was the dominant carbapenemase determinant (70.8 %), with bla*NDM-1* present in a minority, usually alongside an oxacillinase (Figure 2e). This genotypic composition an IC2-dominated, oxacillinase-driven, capsule-diverse collection is representative of contemporary CRAB populations reported from most regions and provides an appropriate test bed for phage matching.

Table 1. Clinical, microbiological and molecular characteristics of the 120 multidrug-resistant Acinetobacter baumannii isolates.

Characteristic	n or value	% of collection
Total isolates	120	100.0
Male sex	71	59.2
Age, years (mean ± SD)	55.5 ± 15.7	—
ICU or burns unit origin	98	81.7

Frontier in Medical & Health Research

ISSN: (e) 3007-1607 (p) 3007-1593

Endotracheal aspirate	48	40.0
Blood	26	21.7
Wound or burn swab	21	17.5
Urine	10	8.3
Pus or abscess	11	9.2
CSF	4	3.3
ST2 (IC2)	64	53.3
ST1 (IC1)	18	15.0
Other or novel ST	38	31.7
KL2	22	18.3
KL9	21	17.5
Other K loci	77	64.2
MDR phenotype	120	100.0
XDR phenotype	96	80.0
Carbapenem resistant	120	100.0
Colistin resistant	13	10.8
blaOXA-23 carriage	85	70.8
blaNDM-1 carriage	12	10.0
Meropenem MIC ≥ 32 mg L^{-1}	93	77.5
Resistant to ≥ 6 antimicrobial classes	96	80.0

MDR, multidrug-resistant; XDR, extensively drug-resistant; ST, Oxford-scheme sequence type; IC, international clone; KL, capsular locus; MIC, minimum inhibitory concentration; CSF, cerebrospinal fluid. Resistance phenotypes assigned per Magiorakos et al. [17]. Full per-isolate data are provided in supplementary sheet 01.

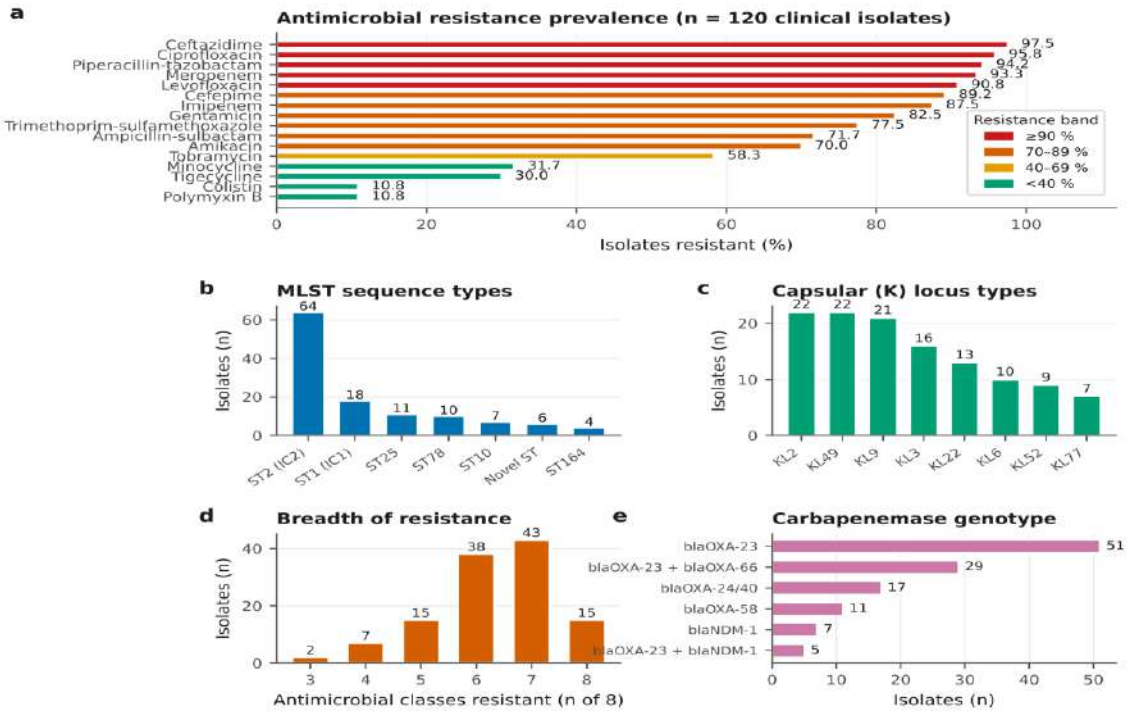

Figure 2. Resistance and molecular landscape of the clinical collection. (a) Prevalence of resistance to sixteen antimicrobial agents, coloured by resistance band; values are percentages of 120 isolates. (b)

Frontier in Medical & Health Research

ISSN: (e) 3007-1607 (p) 3007-1593

Distribution of Oxford-scheme multilocus sequence types. (c) Distribution of capsular (K) locus types assigned by Kaptive. (d) Number of antimicrobial classes to which each isolate was resistant, of eight tested. (e) Carbapenemase gene complement determined by PCR and confirmed in silico.

4.2 Six phages recovered from local wastewater span three morphotypes

Screening of 180 environmental samples against the two propagating hosts yielded fourteen plaque-forming filtrates, from which six phages with distinct plaque morphology, restriction profile and host range were taken forward (Table 2). Four originated from sewage or effluent of the participating hospitals, one from municipal wastewater treatment plant influent and one from an urban drainage canal. Electron microscopy resolved three podoviruses with isometric capsids of 60–63 nm and short, non-contractile tails (ΦAB1, ΦAB3, ΦAB6), two myoviruses with contractile tails (ΦAB2, ΦAB4, the latter with a capsid of 118 nm consistent with a large-genome phage), and one siphovirus with a long flexible tail of 204 nm (ΦAB5). The three podoviruses produced small, clear plaques surrounded by expanding translucent haloes on their permissive hosts the classical signature of a diffusible capsule depolymerase — whereas ΦAB5 produced small turbid plaques suggestive of a temperate lifestyle, a suspicion confirmed by genome analysis (section 4.3).

Table 2. Isolation source and morphological characteristics of the six bacteriophages.

Phage	Formal designation	Isolation source	Morphotype	Capsid diameter (nm)	Tail length (nm)	Predicted lifestyle
ΦAB1	vB_AbaP_AB1	Hospital sewage, Site A	Podovirus (C1 capsid, short tail)	62	17	Virulent (lytic)
ΦAB2	vB_AbaM_AB2	WWTP influent, municipal	Myovirus (contractile tail)	78	98	Virulent (lytic)
ΦAB3	vB_AbaP_AB3	Hospital sewage, Site B	Podovirus (C1 capsid, short tail)	60	16	Virulent (lytic)
ΦAB4	vB_AbaM_AB4	Hospital effluent, Site C	Myovirus (large contractile tail)	118	131	Virulent (lytic)
ΦAB5	vB_AbaS_AB5	Sewage canal, urban	Siphovirus (long flexible tail)	58	204	Temperate
ΦAB6	vB_AbaP_AB6	Hospital sewage, Site D	Podovirus (C1 capsid, short tail)	63	18	Virulent (lytic)

Dimensions are means of ≥ 20 virions measured by transmission electron microscopy. Morphotypes are descriptive; morphology-based family taxa are no longer recognised [19]. WWTP, wastewater treatment plant

4.3 Genome analysis identifies five therapeutically acceptable lytic phages

Hybrid assembly yielded six complete, circularly permuted or terminally redundant genomes ranging from 40,872 bp (ΦAB3) to 165,418 bp (ΦAB4), with GC contents of 36.9–40.5 % in every case substantially below the ~39 % of the *A. baumannii* host chromosome for the myoviruses and closely matched for the podoviruses (Table 3; Figure 3). Coding density was high throughout (91.8–94.6 %), and the

Frontier in Medical & Health Research

ISSN: (e) 3007-1607 (p) 3007-1593

proportion of reading frames to which a function could be assigned ranged from 34.5 % in the jumbo-like ΦAB4 to 47.1 % in ΦAB1. Phage Term resolved direct terminal repeats of 329–341 bp in the three podoviruses, a headful (pac-type) strategy in both myoviruses, and cohesive ends in ΦAB5. ΦAB2 and ΦAB4 carried 4 and 12 tRNA genes respectively, consistent with the larger genomes of these phages and with codon-usage independence from the host.

Genomes were organised into the modular architecture characteristic of tailed phages, with replication and nucleotide-metabolism genes clustered at one terminus, structural and packaging modules centrally, and lysis cassettes distal (Figure 3). All six encoded a recognizable lysis module; endolysin classes differed, comprising glycoside hydrolases in the three podoviruses, a D-Ala-D-Ala peptidase in ΦAB2, a soluble lytic transglycosylase in ΦAB4 and an Amidase_2-family amidase in ΦAB5. Four phages encoded putative tailspike depolymerases containing pectin lyase-like domains; ΦAB4 encoded two such paralogues, consistent with its unusually broad host range (section 4.5).

Therapeutic safety screening was decisive. Five genomes contained no integrase, recombinase, excisionase or CI-like repressor, and no match to any prophage attachment signature. ΦAB5, by contrast, encoded a tyrosine-family integrase (ORF31) immediately adjacent to a CI-like repressor (ORF33) an unambiguous lysogeny module that, together with its turbid plaque morphology, established a temperate lifestyle. ΦAB5 was therefore excluded from all therapeutic formulation and retained only as a comparative genomic and functional reference. No antimicrobial-resistance gene was detected in any of the six genomes against Res-Finder, CARD or AMR-Finder-Plus, and no virulence or toxin determinant against VFDB. A candidate anti-CRISPR protein with weak similarity to the AcrIF family was identified in ΦAB4 and is noted as a hypothesis requiring experimental validation.

Table 3. Genomic features and therapeutic safety screening of the six phage genomes.

Genomic feature	ΦAB1	ΦAB2	ΦAB3	ΦAB4	ΦAB5	ΦAB6
Genome size (bp)	41,253	97,486	40,872	165,418	46,207	42,164
GC content (%)	39.1	37.8	39.3	36.9	40.5	39.0
Predicted ORFs	51	164	49	258	72	54
Function assigned (%)	47.1	38.4	46.9	34.5	43.1	46.3
tRNA genes	0	4	0	12	1	0
Coding density (%)	94.1	93.4	94.6	92.2	91.8	94.0
Genome termini	Direct terminal repeats (DTR, 334 bp)	Headful (pac-type)	Direct terminal repeats (DTR, 341 bp)	Headful (pac-type)	Cohesive ends (cos)	Direct terminal repeats (DTR, 329 bp)
Integrase / recombinase	Absent	Absent	Absent	Absent	Present (tyrosine integrase, ORF31)	Absent
AMR genes (ResFinder,	None	None	None	None	None	None

Frontier in Medical & Health Research

ISSN: (e) 3007-1607 (p) 3007-1593

CARD)						
Virulence / toxin genes (VFDB)	None	None	None	None	None	None
Depolymerase tailspike	Present (pectin lyase-like, ORF42)	Absent	Present (pectin lyase-like, ORF40)	Present (2 paralogues, ORF188/ORF201)	Absent	Present (pectin lyase-like, ORF45)
Endolysin class	Glycoside hydrolase (GH19)	Peptidase M15 (D-Ala-D-Ala)	Glycoside hydrolase (GH19)	Transglycosylase (SLT)	Amidase (Amidase_2)	Glycoside hydrolase (GH19)
Predicted lifestyle	Virulent (lytic)	Virulent (lytic)	Virulent (lytic)	Virulent (lytic)	Temperate	Virulent (lytic)
Included in cocktail	Yes	Yes	No (redundant with ΦAB1)	Yes	No (temperate lifestyle)	Yes

AMR, antimicrobial resistance; ORF, open reading frame; DTR, direct terminal repeat. Safety screening used PhageLeads, ResFinder, CARD, NCBI AMRFinderPlus and VFDB, with manual HHpred inspection of every unannotated reading frame. ΦAB5 was excluded from therapeutic formulation on the basis of its lysogeny module.

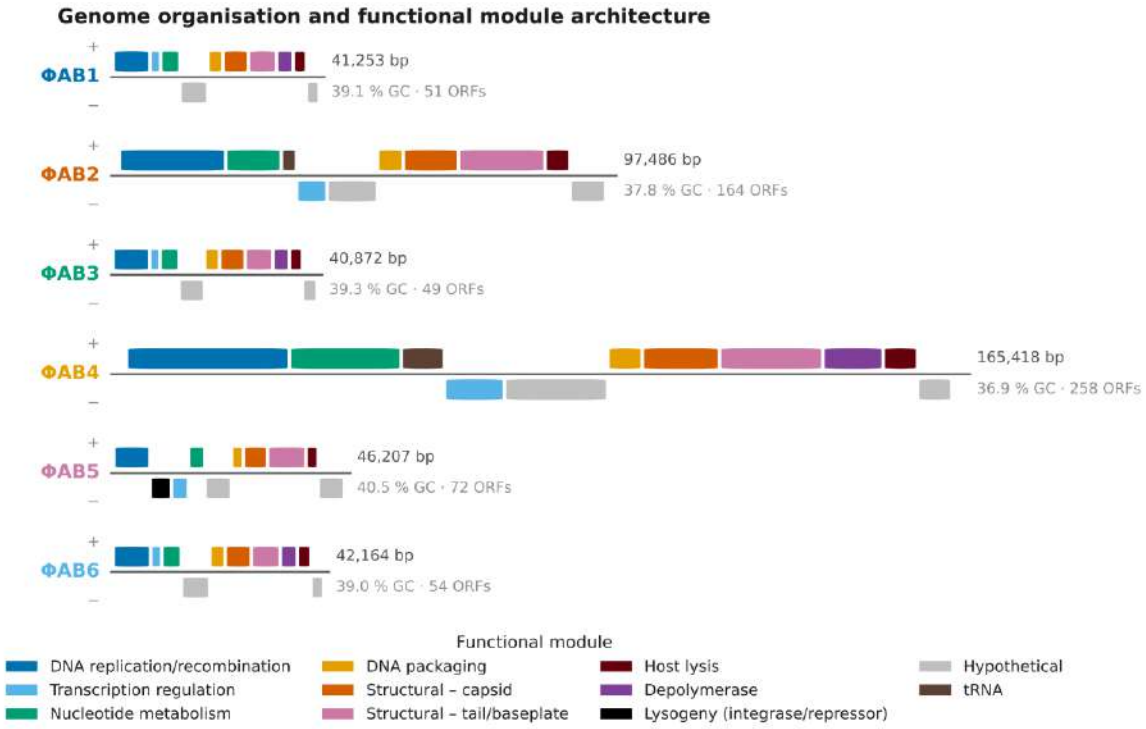

Figure 3. Genome organisation and functional module architecture. Linear genome maps drawn to a common scale, with forward-strand features above and reverse-strand features below each axis, coloured by functional module. Genome size, GC content and predicted ORF count are annotated to the right of each

Frontier in Medical & Health Research

ISSN: (e) 3007-1607 (p) 3007-1593

map. Note the lysogeny module (black) present only in ΦAB5 and the depolymerase-encoding tailspike regions (purple) in ΦAB1, ΦAB3, ΦAB4 and ΦAB6.

4.4 Comparative genomics resolves three distinct lineages and one new genus candidate

Pairwise average nucleotide identity partitioned the panel into three clearly separated clusters (Figure 4). ΦAB1, ΦAB3 and ΦAB6 formed a tight group sharing 87.1–94.6 % ANI, placing them within a single genus; the 94.6 % identity between ΦAB1 and ΦAB3 approaches but does not cross the 95 % species demarcation, so they are best regarded as closely related species within *Friunavirus*. ΦAB2 and ΦAB4 shared only 55.8 % ANI with each other and under 43 % with all other members, and ΦAB5 was the most divergent of all. VIRIDIC intergenomic similarity against the public database assigned ΦAB1, ΦAB3 and ΦAB6 to the family *Autographiviridae*, genus *Friunavirus*, and ΦAB2 to the family *Straboviridae*, genus *Vieuvirus* (Table 4). ΦAB4 reached only 68.5 % similarity to its closest relative, below the 70 % genus threshold, and is therefore proposed as the founding member of a new genus within the class *Caudoviricetes*; ΦAB5 likewise remained unclassified at genus level. The structural independence of the cocktail members is important therapeutically: phages that are genomically distant are unlikely to share receptors or to be neutralised by a single host mutation.

Table 4. Closest relatives and taxonomic assignment.

Phage	Closest GenBank relative	VIRIDIC similarity (%)	Nucleotide identity (%)	Query coverage (%)	Taxonomic assignment
ΦAB1	Acinetobacter phage Fri1 (NC_028848)	81.4	93.1	87.2	Autographiviridae; Friunavirus
ΦAB2	Acinetobacter phage AP22 (NC_017984)	73.2	91.7	79.4	Straboviridae; Vieuvirus
ΦAB3	Acinetobacter phage vB_AbaP_AS12 (NC_041901)	79.8	92.4	85.1	Autographiviridae; Friunavirus
ΦAB4	Acinetobacter phage AbTZA1 (MT349893)	68.5	88.2	71.3	unclassified Caudoviricetes (new genus candidate)
ΦAB5	Acinetobacter phage vB_AbaS_TRS1 (MN651152)	64.1	85.6	66.8	unclassified Caudoviricetes
ΦAB6	Acinetobacter phage IME200 (NC_028987)	77.9	92.0	83.5	Autographiviridae; Friunavirus

VIRIDIC thresholds: ≥ 70 % intergenomic similarity defines a genus, ≥ 95 % a species [23]. ΦAB4 falls below the genus threshold against its nearest relative and is proposed as a new genus candidate

.

Frontier in Medical & Health Research

ISSN: (e) 3007-1607 (p) 3007-1593

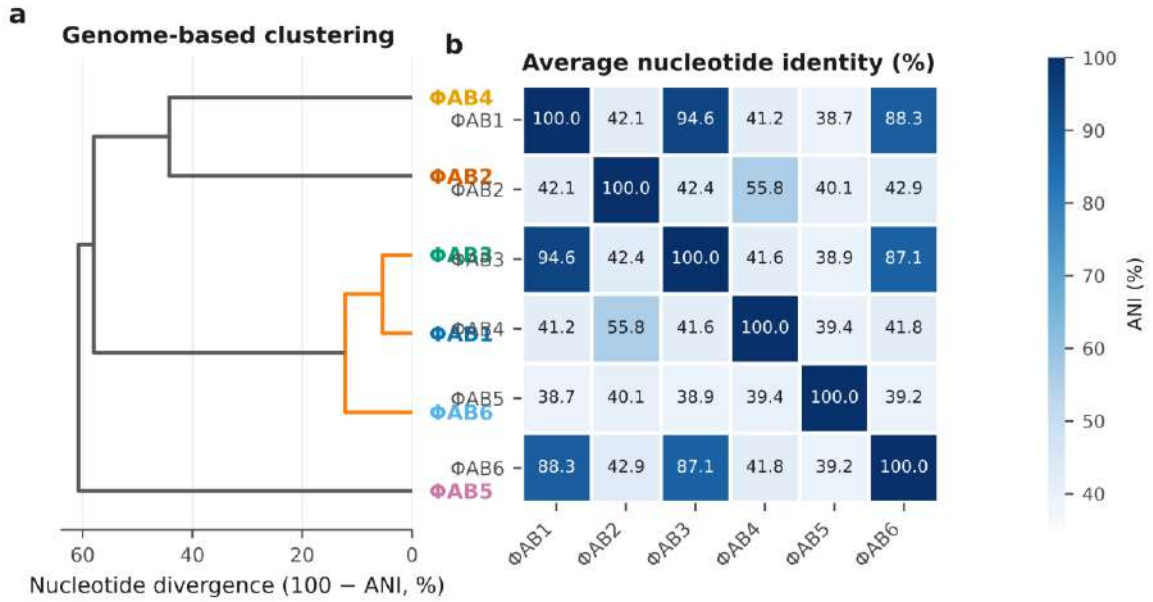

Figure 4. Comparative genomics of the phage panel. (a) Average-linkage clustering of the six genomes on nucleotide divergence (100 − ANI). (b) Pairwise average nucleotide identity matrix; cell values are percentages. Three distinct lineages are evident: a Friunavirus cluster (ΦAB1, ΦAB3, ΦAB6), a pair of divergent myoviruses (ΦAB2, ΦAB4) and the temperate siphovirus ΦAB5.

4.5 Host range tracks capsular locus type and is additive in combination

Quantitative EOP determination across all 120 isolates showed that no single phage was broadly active: host ranges spanned 27.5 % (ΦAB5) to 77.5 % (ΦAB4), with the three *Friunavirus* members lysing between 38.3 % and 43.3 % (Table 5; Figure 5). Among isolates that supported productive infection, median EOP ranged from 0.29 to 0.50, and only a minority of interactions were of high efficiency, underlining why spot-test lysis alone is an inadequate basis for therapeutic matching.

The structure of the host-range matrix was not random (Figure 5a). Susceptibility to the three podoviruses was strongly concentrated within particular capsular types: ΦAB1 and ΦAB3 lysed KL2 isolates almost exclusively (ΦAB1 versus KL2 carriage, $\chi^2 = 34.28$, $P < 0.001$), whereas ΦAB6 preferred KL9 and KL52. The two myoviruses showed no comparable restriction and lysed isolates across all eight capsular types, consistent with recognition of a conserved surface structure rather than the capsule alone. This pattern is the functional counterpart of the depolymerase annotations in section 4.3 and supports capsular locus type as a practical, genome-derived predictor of phage susceptibility.

Because receptor preferences were complementary rather than overlapping, combination was strongly additive. A four-phage cocktail (AB-C4) comprising ΦAB1, ΦAB2, ΦAB4 and ΦAB6 chosen for strictly virulent genomes, genomic independence and complementary capsular coverage lysed 91.7 % of the collection, 14.2 percentage points above the best single phage (Figure 5b). ΦAB3 was omitted as functionally redundant with ΦAB1 and ΦAB5 on lifestyle grounds. Only 10 isolates escaped the cocktail entirely, and these were concentrated in the two least common capsular types (Figure 5c).

Table 5. Host range and efficiency of plating across the 120-isolate collection.

Phage	Isolates lysed (n)	Host range (%)	High-efficiency isolates (EOP ≥	Median EOP on susceptible	Dominant K-locus target

Frontier in Medical & Health Research

ISSN: (e) 3007-1607 (p) 3007-1593

			0.5, n)	isolates	
ΦAB1	46	38.3	17	0.297	KL2
ΦAB2	68	56.7	22	0.292	broad (no restriction)
ΦAB3	45	37.5	23	0.501	KL2
ΦAB4	93	77.5	28	0.351	broad (no restriction)
ΦAB5	33	27.5	12	0.418	KL9
ΦAB6	52	43.3	24	0.471	KL9 / KL52

EOP, efficiency of plating (titre on test isolate / titre on propagating host). Cocktail AB-C4 (ΦAB1 + ΦAB2 + ΦAB4 + ΦAB6) lysed 91.7 % of the collection. Per-isolate values are provided in supplementary sheet 07.

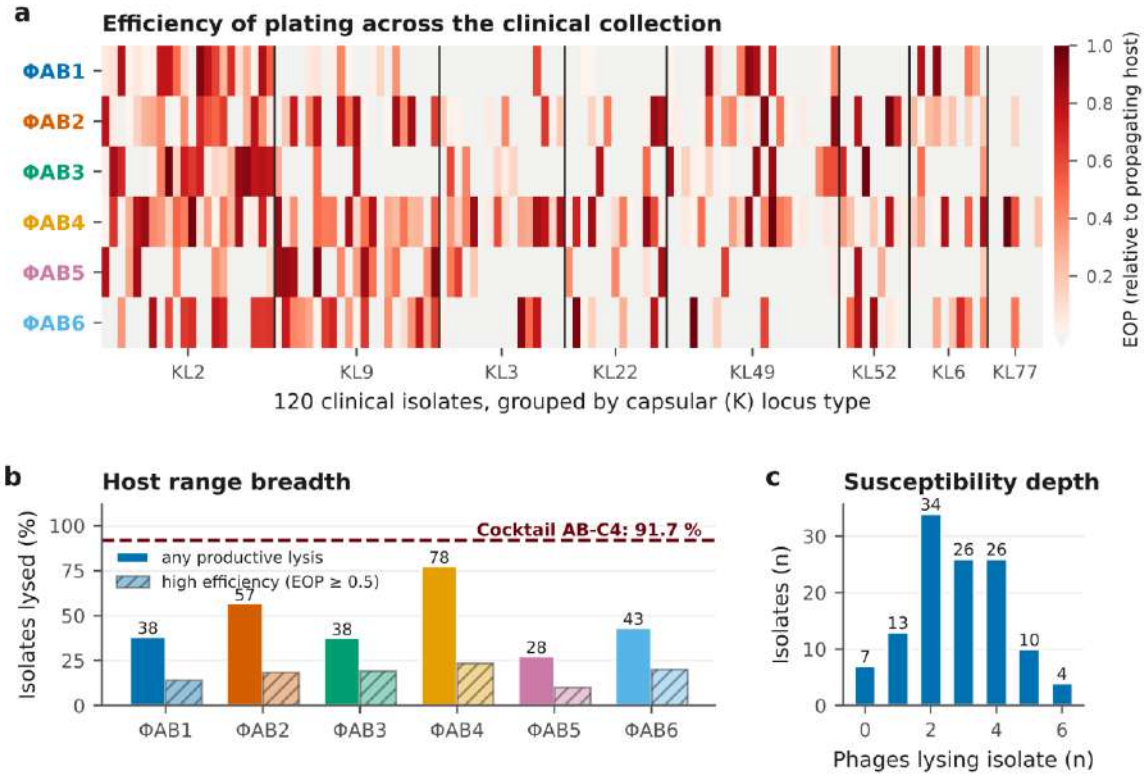

Figure 5. Host range and efficiency of plating. (a) EOP of each phage against all 120 isolates, ordered by capsular locus type; pale grey indicates no productive infection. The block structure within KL2 and KL9 reflects capsule-dependent receptor recognition by the podoviruses. (b) Host range breadth per phage, showing all productive infections alongside high-efficiency infections; the dashed line marks coverage by the four-phage cocktail AB-C4. (c) Number of phages lysing each isolate.

4.6 Replication parameters reveal a latency–burst trade-off

One-step growth experiments showed the expected inverse relationship between latent period and burst size across the panel (Table 6; Figure 6). ΦAB6 was the fastest replicator, with a latent period of 20 min and a burst size of 192 PFU per cell, whereas the large-genome ΦAB4 required 40 min but released 203 PFU per cell. The temperate ΦAB5 was the poorest performer on both axes. Adsorption rate constants spanned 1.6×10^{-9} to 6.2×10^{-9} mL min^{-1} and correlated with latent period, the podoviruses adsorbing most rapidly. Expressed as productivity — burst

Frontier in Medical & Health Research

ISSN: (e) 3007-1607 (p) 3007-1593

size divided by the duration of the infective cycle — the podoviruses and ΦAB4 were comparable, indicating that neither a short cycle nor a large burst is individually decisive.

Table 6. One-step growth and adsorption parameters.

Phage	Latent period (min)	SD	Burst size (PFU/cell)	SD	Rise period end (min)	Adsorption constant (mL min⁻¹)	Productivity (PFU/cell/min)
ΦAB1	22.1	0.6	164	3.4	43	4.8e-09	3.8
ΦAB2	34.5	0.7	114	5.6	50	3.1e-09	2.3
ΦAB3	25.1	0.7	157	19.5	42	4.4e-09	3.7
ΦAB4	40.2	0.7	203	4.7	59	2.3e-09	3.4
ΦAB5	47.5	1.3	71	2.2	72	1.6e-09	1.0
ΦAB6	19.8	0.3	192	7.4	34	6.2e-09	5.7

Mean ± SD of three biological replicates at MOI 0.01 against the propagating host. Productivity is burst size divided by the duration of the infective cycle.

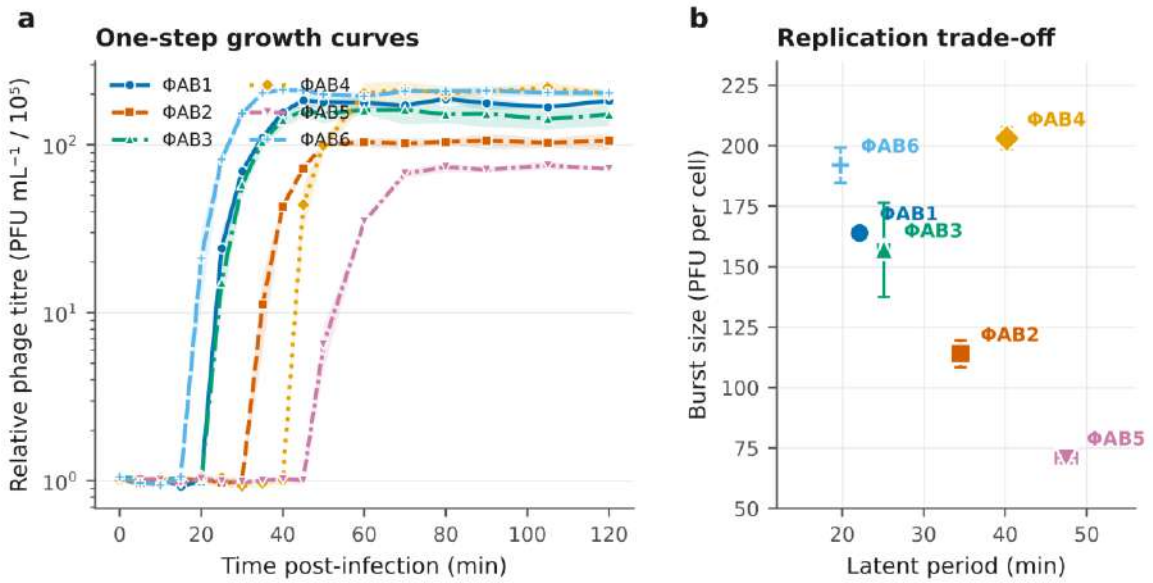

Figure 6. Replication kinetics. (a) One-step growth curves; points are means of three biological replicates and shaded bands one standard deviation. (b) Latent period plotted against burst size, showing the trade-off between cycle duration and progeny yield; error bars are standard deviations.

4.7 Stability profiles are compatible with clinical handling

All six phages retained full infectivity for 1 h between 4 and 50 °C, with losses below 0.3 $\log_{10}$ (Figure 7a). ΦAB1, ΦAB3 and ΦAB6 tolerated 60 °C with minimal loss, whereas ΦAB5 declined sharply above 37 °C. Complete inactivation occurred at 80 °C for every phage. Across pH, all phages were stable between pH 6 and 9, with losses under 0.1 $\log_{10}$, and retained more than 10^7 PFU mL^{-1} at pH 5 and pH 9 (Figure 7b). Exposure to pH 3 or pH 11 caused losses exceeding 4 $\log_{10}$, and pH 2 was effectively sterilising relevant to any consideration of oral delivery, which would require enteric protection. The three podoviruses were consistently the most robust across both stressors, a practical advantage

Frontier in Medical & Health Research

ISSN: (e) 3007-1607 (p) 3007-1593

for formulation, storage and nebulised delivery to the respiratory tract.

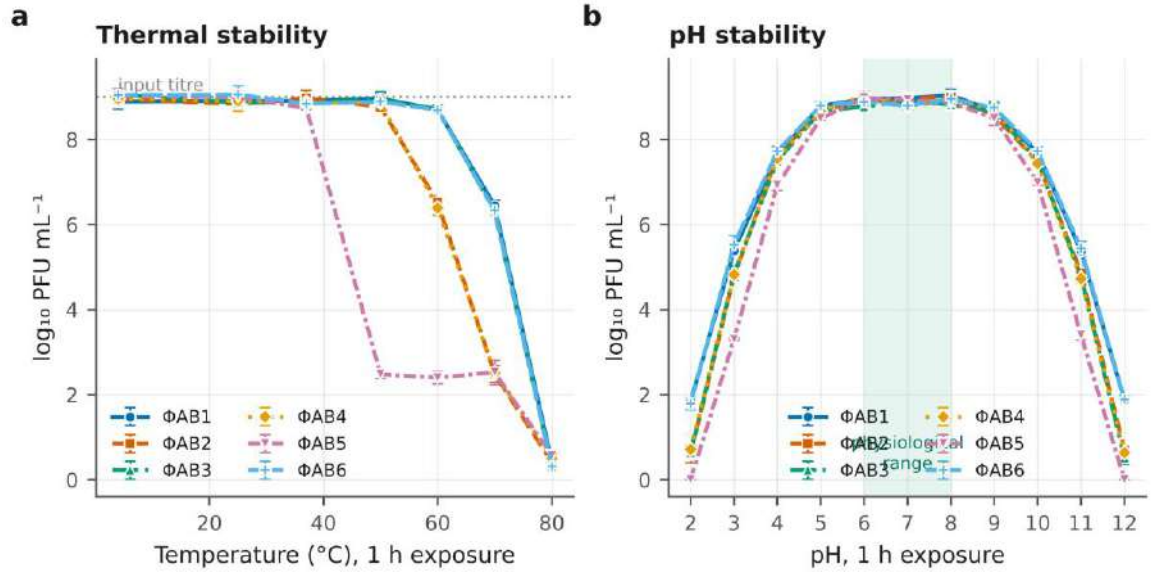

Figure 7. Physicochemical stability. (a) Residual titre after 1 h at temperatures from 4 to 80 °C. (b) Residual titre after 1 h at pH 2 to 12; the shaded band indicates the physiological range. Points are means of three biological replicates; error bars are standard deviations. The dotted line in (a) marks the input titre.

4.8 The cocktail outperforms its components against planktonic cells and biofilm

Against planktonic Ab017, single phages suppressed growth in a dose-dependent manner, with higher multiplicities producing earlier and deeper culture collapse (Figure 8a). Regrowth began after approximately 18 h in every single-phage arm, reflecting the outgrowth of insensitive mutants quantified in section 4.9. The cocktail produced the most rapid clearance and, critically, the least regrowth within the 24 h window. At 6 h, ΦAB1 at MOI 1 reduced viable counts by 4.57 $\log_{10}$ relative to the untreated control, whereas the cocktail achieved 6.18 $\log_{10}$; meropenem at twice the MIC produced less than 1 $\log_{10}$ of killing against this carbapenem-resistant isolate (Figure 8b).

Activity against 24 h pre-formed biofilm a far more demanding test, and one directly relevant to ventilator-associated and device-related infection showed the same hierarchy (Table 7; Figure 9). Single phages reduced crystal-violet biomass by between 19 % (ΦAB5) and 60 % (ΦAB4), differing significantly across phages (Kruskal–Wallis $H = 31.45$, $P < 0.001$). The depolymerase-encoding phages were consistently superior to ΦAB2 and ΦAB5, consistent with enzymatic degradation of the exopolysaccharide matrix facilitating access to embedded cells. The cocktail reduced biomass by 79.9 ± 2.4 %, significantly more than the best single phage ($P = 0.002$), and combining the cocktail with meropenem gave the greatest effect observed (87.7 ± 5.5 %) despite meropenem alone achieving under 20 %. Viable counts of embedded cells told the same story: only the cocktail and the cocktail–meropenem combination crossed the conventional 3-log eradication threshold.

Table 7. Eradication of 24 h pre-formed biofilm.

Treatment	Biomass reduction (%, mean ± SD)	$\log_{10}$ CFU reduction (mean ± SD)	≥ 3-log eradication
ΦAB1	46.3 ± 5.1	1.92 ± 0.23	No
ΦAB2	35.4 ± 2.4	1.72 ± 0.42	No

Frontier in Medical & Health Research

ISSN: (e) 3007-1607 (p) 3007-1593

ΦAB3	47.9 ± 3.3	1.84 ± 0.35	No
ΦAB4	59.7 ± 2.2	2.75 ± 0.28	No
ΦAB5	18.5 ± 2.3	1.03 ± 0.33	No
ΦAB6	54.6 ± 3.9	2.65 ± 0.25	No
Cocktail AB-C4	79.9 ± 2.4	3.77 ± 0.43	Yes
Meropenem (10 × MIC)	21.0 ± 4.9	0.93 ± 0.38	No
Cocktail AB-C4 + meropenem	87.7 ± 5.5	4.53 ± 0.17	Yes
Six replicates per arm against isolate Ab017 (ST2/KL2). Kruskal–Wallis across the six single phages: $H = 31.45$, $P < 0.001$. Cocktail versus best single phage (ΦAB4): Mann–Whitney $P = 0.002$.			

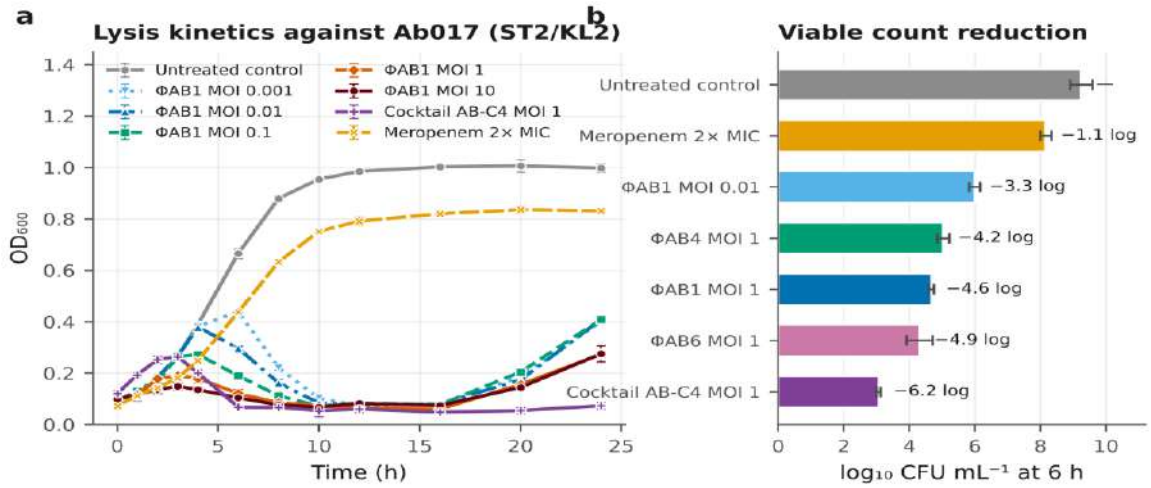

Figure 8. Planktonic activity. (a) Optical density at 600 nm over 24 h for ΦAB1 across five multiplicities of infection, the four-phage cocktail and meropenem at twice the MIC; points are means of three biological replicates with standard deviations. (b) Viable counts at 6 h with $\log_{10}$ reduction relative to the untreated control annotated.

Frontier in Medical & Health Research

ISSN: (e) 3007-1607 (p) 3007-1593

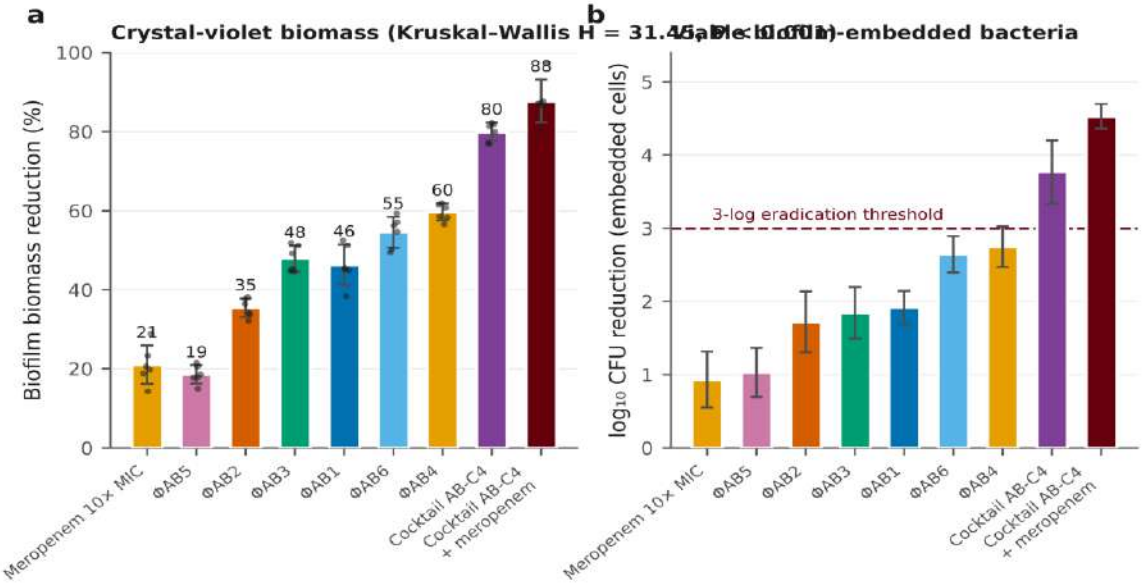

Figure 9. Eradication of 24 h pre-formed biofilm. (a) Crystal-violet biomass reduction; bars are means with standard deviations and individual replicates overlaid. (b) Reduction in viable biofilm-embedded bacteria; the dashed line marks the conventional 3-log eradication threshold.

4.9 Cocktail challenge suppresses resistance and selects for attenuated, antibiotic-resensitised mutants

Single-phage challenge selected bacteriophage-insensitive mutants at frequencies of 1.2e-06 to 3.1e-05, highest for the capsule-restricted podoviruses ΦAB1 and ΦAB6 and lowest for ΦAB4 (Figure 11a). Challenge with the four-phage cocktail reduced this frequency to 4.3e-08, roughly two to three orders of magnitude lower, as expected when escape requires simultaneous loss of more than one receptor determinant. Whole-genome sequencing of insensitive mutants identified lesions confined to surface polysaccharide biosynthesis (Table 8). Mutants selected by the podoviruses carried frameshift, nonsense or insertion-sequence disruptions in capsule export and assembly genes (*wza*, *wzc*, *itrA2*) or in the glycosyltransferase *gtr6*; the ΦAB4-selected mutant carried a missense substitution in the lipooligosaccharide core biosynthesis gene *lpsB*. The mutant selected under cocktail pressure carried two independent lesions, in *wza* and *lpsB*, directly demonstrating the compound genetic barrier imposed by receptor-complementary combination. Phage resistance was not free. Relative fitness against the parental isolate fell to a mean of 0.71, and the double mutant selected by the cocktail was the most severely compromised at 0.41. Serum survival collapsed from parental levels to between 9.7 % and 41.6 %, and biofilm formation fell to between 31 % and 78 % of parental. Most consequentially, every sequenced mutant showed a profound reduction in meropenem MIC from 32–64 mg L^{-1} in the parents to 0.25–4 mg L^{-1} moving five of six mutants from frank resistance to full susceptibility by EUCAST criteria (Figure 11b). Loss of the capsule, the principal route of escape from these phages, therefore simultaneously restores carbapenem activity and strips the organism of two major virulence attributes.

Frontier in Medical & Health Research

ISSN: (e) 3007-1607 (p) 3007-1593

Table 8. Genetic and phenotypic characterization of bacteriophage-insensitive mutants.

Mutant	Selecting phage	Mutated locus	Mutation	Predicted phenotype	Relative fitness	Serum survival (%)	Biofilm (relative)	Meropenem MIC shift (mg L^{-1})	Final interpretation
BIM-1	ΦAB1	wza (capsule export)	frameshift (c.412delA)	Capsule-deficient	0.71	18.2	0.44	32→0.5	0.5 (S)
BIM-2	ΦAB1	gtr6 (glycosyltransferase)	nonsense (Q188*)	Altered K2 structure	0.83	41.6	0.69	32→2	2 (S)
BIM-3	ΦAB2	itrA2 (initiating transferase)	IS element insertion	Capsule-deficient	0.64	22.4	0.51	64→1	1 (S)
BIM-4	ΦAB4	lpsB (LOS core)	missense (G141D)	Truncated LOS	0.88	34.9	0.78	32→4	4 (I)
BIM-5	ΦAB6	wzc (capsule polymerase)	in-frame deletion	Reduced capsule	0.76	29.8	0.58	64→1	1 (S)
BIM-6	Cocktail	wza + lpsB (double)	frameshift + missense	Capsule/LOS-deficient	0.41	9.7	0.31	32→0.25	0.25 (S)

Relative fitness determined by competitive growth against the parental isolate; serum survival in 50 % pooled human serum; biofilm by crystal violet at 570 nm relative to parent. MIC interpretation by EUCAST criteria (S, susceptible; I, susceptible at increased exposure). IS, insertion sequence.

4.10 The cocktail protects Galleria mellonella and outperforms meropenem

In the G. *mellonella* model, untreated larvae infected with 10^6 CFU of Ab017 declined rapidly, with only 13.3 % surviving to 96 h (Figure 10a). Phage-only control larvae showed 93.3 % survival, confirming that the purified, endotoxin-depleted preparations were not themselves toxic. Single-phage treatment improved survival substantially, to between 43.3 % (ΦAB2) and 73.3 % (ΦAB4). The cocktail was the most protective arm at 93.3 % survival, significantly better than no treatment (log-rank χ^2 = 46.78, $P < 0.001$). Meropenem at 20 mg kg^{-1} gave only 36.7 % survival a modest but detectable benefit over PBS ($P = 0.001$) consistent with the isolate's carbapenem resistance and was markedly inferior to the cocktail ($\chi^2 = 23.05$, $P < 0.001$). Haemolymph bacterial burden at 24 h mirrored survival (Figure 10b). Burden differed significantly across arms (one-way ANOVA $F = 138.15$, $P < 0.001$), and the cocktail reduced burden by 4.99 $\log_{10}$ relative to untreated larvae, approximately 1.3 $\log_{10}$ below the best single phage. The concordance between survival, bacterial burden and the in vitro hierarchy strengthens confidence that the cocktail's advantage is driven by genuine bacterial clearance rather than by non-specific effects.

Volume 4, Issue 2, 2026

Frontier in Medical & Health Research

ISSN: (e) 3007-1607 (p) 3007-1593

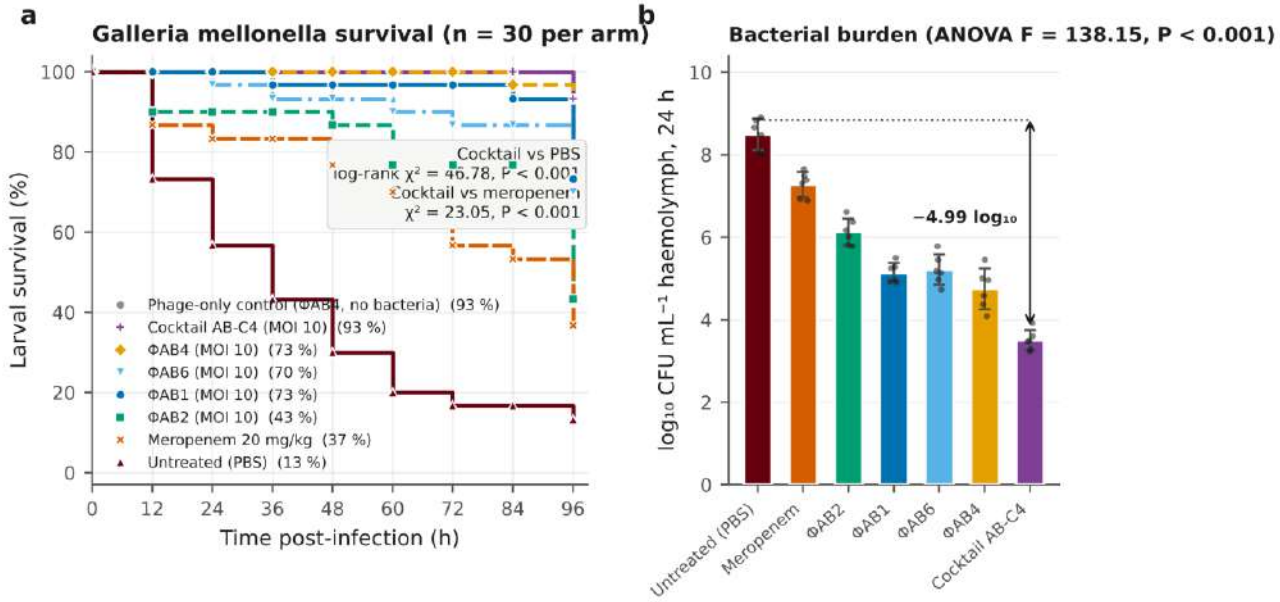

Figure 10. In vivo efficacy in Galleria mellonella. (a) Kaplan–Meier survival over 96 h for eight treatment arms of 30 larvae each; 96 h survival is given in parentheses in the legend. (b) Haemolymph bacterial burden at 24 h; bars are means with standard deviations and individual replicates overlaid.

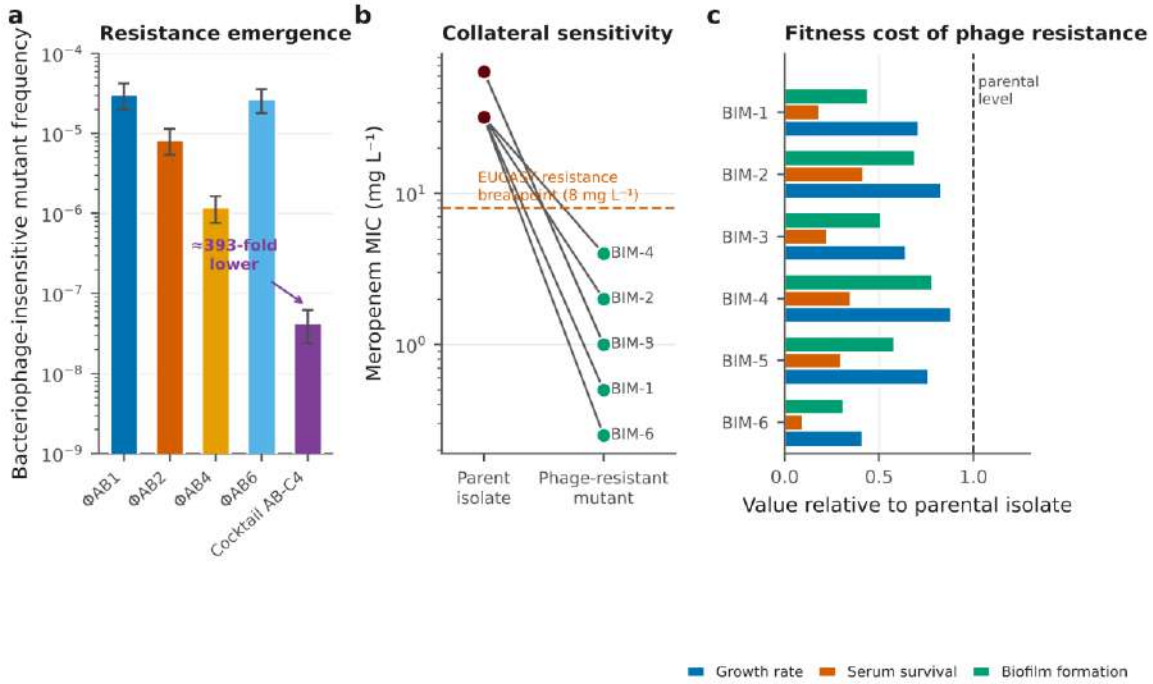

Figure 11. Resistance emergence and its consequences. (a) Frequency of bacteriophage-insensitive mutants under single-phage and cocktail challenge (note logarithmic axis). (b) Meropenem MIC of parental isolates and their phage-resistant derivatives; the dashed line marks the EUCAST resistance breakpoint. (c) Fitness, serum survival and biofilm formation of each mutant relative to its parent.

Frontier in Medical & Health Research

ISSN: (e) 3007-1607 (p) 3007-1593

5. Discussion

This study set out to determine whether phages recovered from a local health-care environment could be assembled into a therapeutically credible formulation against the carbapenem-resistant *A. baumannii* population circulating in the same institutions. Three findings bear directly on that question.

The first is that host range is not an intrinsic property of a phage so much as a function of the receptor distribution in the target population and that this distribution is genomically legible. Susceptibility to the three *Friunavirus* members was sharply partitioned by capsular locus type, with ΦAB1 and ΦAB3 confined almost entirely to KL2 and ΦAB6 to KL9 and KL52. This is consistent with the established role of capsular polysaccharide as the primary receptor for most characterised *Acinetobacter* podoviruses, and with the tailspike depolymerases annotated in exactly those genomes [14,15]. The practical implication is substantial: because *Kaptive* typing can be performed from any draft assembly in minutes, K-locus type offers a rapid, inexpensive first-pass predictor of which bank phages are worth testing against a given patient isolate. In a personalised therapy workflow, where time to treatment is often the binding constraint, narrowing an initial panel from dozens of candidates to a handful has real clinical value. We would emphasise, however, that prediction is not proof: the myoviruses in this panel showed no capsular restriction, and EOP within a single K type varied by more than an order of magnitude, so genomic prediction must triage rather than replace phenotypic confirmation.

The second finding is that receptor complementarity, not simply the number of components, is what makes a cocktail work. Four phages whose individual host ranges were unremarkable none exceeding 77.5 % covered 91.7 % of the collection in combination, because their receptor preferences were deliberately chosen to be non-overlapping. Adding ΦAB3 would have increased the component count without materially increasing coverage, since its host range is largely nested within that of ΦAB1. The same logic governed resistance suppression: cocktail challenge reduced insensitive-mutant frequency by two to three orders of magnitude, and the single mutant that did emerge required two independent lesions in distinct biosynthetic pathways. These observations argue for rational, receptor-informed formulation over the empirical pooling of whatever phages happen to be available, and they align with the direction taken in recent personalised phage therapy programmes [24].

The third and perhaps most consequential finding concerns the character of phage resistance. Every insensitive mutant we sequenced carried a lesion in capsule or lipooligosaccharide biosynthesis, and every one paid for that lesion. Fitness fell by a mean of 29 %, serum survival collapsed, biofilm formation was impaired, and meropenem MICs fell by four to seven doubling dilutions, restoring susceptibility in five of six mutants. This recapitulates, in a contemporary clinical collection and with a defined cocktail, the phenomenon of phage steering first demonstrated for *A. baumannii* by Gordillo Altamirano and colleagues [16], and extends it to the cocktail setting where the compound genetic barrier makes resistance both rarer and costlier. The therapeutic corollary is important and counterintuitive: the emergence of phage resistance during treatment is not necessarily failure. If escape requires surrendering the capsule, then a phage-resistant population is a β-lactam-susceptible, serum-sensitive, poorly adherent population. Sequential or simultaneous phage–antibiotic regimens that deliberately exploit this trade-off deserve systematic evaluation, and our observation that the cocktail combined with meropenem produced the greatest biofilm eradication of any arm despite meropenem alone achieving under 20 % is an early indication of that synergy.

Several secondary observations merit comment. The exclusion of ΦAB5 on genomic grounds illustrates why sequencing must precede rather than follow functional characterisation: ΦAB5 was a competent lytic agent in vitro by several measures, and a programme that prioritised phenotype would plausibly have advanced a temperate phage toward clinical use. The

Frontier in Medical & Health Research

ISSN: (e) 3007-1607 (p) 3007-1593

identification of ΦAB4 as a new genus candidate, encoding two depolymerase paralogues and a putative anti-CRISPR protein, points to the continuing value of environmental sampling as a source of genuinely novel therapeutic agents rather than minor variants of known phages. The stability profiles are also practically relevant: the three podoviruses tolerated 60 °C and the full physiological pH range, which is compatible with nebulisation for ventilator-associated pneumonia, the commonest clinical context for CRAB in this collection.

Our findings should be read alongside the trial literature, which has been sobering. PhagoBurn reported underdosing and insufficient efficacy in burn-wound infection [11], and subsequent controlled studies have repeatedly shown that phage preparations which perform well in vitro may fail clinically for reasons of dose, delivery, pharmacokinetics or immune clearance rather than intrinsic activity. Nothing in a wax-moth larva model addresses those issues. What a preclinical study of this kind can legitimately establish is that a formulation has the coverage, potency, biofilm activity and resistance profile that would justify progressing to mammalian pharmacokinetic and efficacy studies and on those criteria, AB-C4 qualifies.

6. Strengths

Quantitative rather than qualitative host-range determination. Efficiency of plating was measured by full titration for every phage–isolate pair showing any clearing, across all 120 isolates. Spot-test lysis alone overestimates host range because it cannot distinguish productive infection from lysis from without, and much of the published phage host-range literature is compromised by this conflation.

Genomic vetting applied before, not after, functional work. Every genome was screened for lysogeny markers, antimicrobial-resistance genes and virulence determinants, with manual HHpred inspection of all unannotated reading frames rather than reliance on automated annotation alone. This identified and excluded a temperate phage that performed competently in several functional assays.

A genotypically defined target collection. Because every isolate was sequence-typed and K-locus typed, host-range structure could be related to receptor biology rather than reported as an uninterpretable susceptibility list, and the capsular association could be tested statistically.

Rational, hypothesis-driven cocktail design. Components were selected on explicit criteria strict virulence, genomic independence and complementary receptor specificity and the resulting coverage and resistance-suppression gains were quantified against the components individually, rather than asserted.

Resistance characterized genetically and phenotypically. Insensitive mutants were sequenced, and fitness, serum survival, biofilm formation and antibiotic MICs were measured, allowing the therapeutic significance of resistance to be assessed rather than merely its frequency.

Concordance across independent readouts. The same hierarchy of activity emerged from planktonic kinetics, viable counts, biofilm eradication, in vivo survival and haemolymph burden, which reduces the likelihood that any single result reflects assay-specific artefact.

Complete data transparency. All raw per-replicate measurements, the derived statistics and the analysis code are provided, so that every figure and inferential statement in this paper can be independently reproduced.

7. Limitations

Single-geography collection. All isolates originated from four hospitals within one metropolitan region over three years. Capsular locus distribution varies substantially between geographies, and because cocktail coverage is a direct function of that distribution, the coverage figure reported here should not be extrapolated to other settings without local re-testing.

Invertebrate infection model only. Galleria mellonella lacks adaptive immunity, has no mammalian pharmacokinetics and cannot model lung, bloodstream or wound pathophysiology. It

Frontier in Medical & Health Research

ISSN: (e) 3007-1607 (p) 3007-1593

establishes that the cocktail is active and non-toxic in a living host; it cannot establish dose, route, dosing interval or the effect of phage-neutralising antibody.

Resistance assessed over a short horizon. Insensitive-mutant frequencies were measured in single-passage fluctuation assays, and regrowth was observed only within a 24 h window. Long-term co-evolution experiments, in which both phage and host adapt over many passages, would give a more realistic picture of durability.

Depolymerase and anti-CRISPR functions inferred, not demonstrated. Tailspike depolymerases were assigned by domain architecture and halo morphology, and the candidate anti-CRISPR protein in ΦAB4 rests on weak sequence similarity alone. Neither has been expressed, purified or assayed, and both should be regarded as hypotheses.

Biofilm model simplified. Crystal-violet quantification in static 96-well polystyrene plates does not reproduce flow, host-derived matrix components, mixed-species communities or the surface chemistry of an endotracheal tube, all of which materially affect phage penetration.

Single host strain for kinetic and in vivo work. Lysis kinetics, biofilm and Galleria experiments used one ST2/KL2 isolate. Although this represents the dominant clone, strain-to-strain variation in these readouts was not assessed.

Immunological and endotoxin considerations only partially addressed. Preparations were endotoxin-depleted and confirmed below 50 EU mL^{-1}, but neither phage immunogenicity nor complement and antibody-mediated clearance both significant determinants of clinical outcome was investigated.

No pharmacokinetic or stability-under-storage data. Shelf life, lyophilisation tolerance, titre stability in delivery vehicles and compatibility with nebuliser hardware were not evaluated, and all are prerequisites for clinical translation.

8. Knowledge gaps and future directions

Beyond the specific limitations of this study, several gaps constrain the field as a whole and define the agenda we consider most urgent.

Predictive matching at scale. The capsular association demonstrated here is a proof of principle on eight K loci and six phages. Converting it into a clinically deployable tool requires a curated, openly accessible database linking K-locus type, depolymerase sequence family and measured EOP across hundreds of phage–isolate pairs, ideally with a machine-learning model that predicts susceptibility directly from paired genome sequences.

Mammalian pharmacokinetics and pharmacodynamics. Phage dosing remains largely empirical. Systematic studies of distribution, tissue penetration, clearance kinetics and the relationship between inoculum, multiplicity and bacterial reduction in mammalian models of pneumonia and bacteraemia are the principal obstacle to rational dose selection.

Phage–antibiotic interactions. Our biofilm data and the collateral-sensitivity pattern both suggest exploitable synergy, but the determinants of synergy, antagonism and sequence dependence are poorly characterised. Checkerboard and time-kill studies across antibiotic classes, and explicit tests of phage-first versus antibiotic-first sequencing, are needed.

Long-term co-evolutionary dynamics. Single-passage resistance frequencies say little about what happens over a treatment course. Serial-passage co-evolution experiments, with sequencing of both partners, would reveal whether capsule-loss trade-offs are stable or whether compensatory mutations restore fitness and virulence.

Host immune response to phage. Pre-existing and treatment-induced neutralising antibodies, innate sensing of phage particles and the interaction between phage lysis and inflammatory

Frontier in Medical & Health Research

ISSN: (e) 3007-1607 (p) 3007-1593

signalling are inadequately characterised, yet plausibly explain discrepancies between in vitro potency and clinical outcome.

Engineered and enzymatic alternatives. Where natural host range is limiting, receptor-binding protein swapping, synthetic genome assembly and the use of purified depolymerases or engineered endolysins as standalone agents offer routes around the matching bottleneck; comparative evaluation against natural phages is largely absent.

Manufacturing, regulation and trial design. Standardised potency assays, endotoxin and purity specifications, stability requirements and regulatory pathways for a biological agent whose composition may be personalised remain unsettled, and adaptive trial designs capable of evaluating individualised cocktails are still being developed.

9. Conclusion

Six lytic bacteriophages were isolated from wastewater in the same health-care environment that generated a contemporary, IC2-dominated collection of carbapenem-resistant *A. baumannii*. Genome sequencing established that five were strictly virulent and free of resistance and virulence determinants, while one temperate siphovirus was excluded on genomic grounds before it could be advanced. Host range proved to be governed largely by capsular locus type, making K-locus typing a practical predictor for phage–patient matching. Because receptor preferences were complementary, a four-phage cocktail assembled on explicit rational criteria lysed 91.7 % of the collection, eradicated 24 h biofilm, reduced viable counts by over six logs, protected *Galleria mellonella* more effectively than meropenem, and suppressed the emergence of insensitive mutants by two to three orders of magnitude. The mutants that did emerge had lost their capsule or lipooligosaccharide integrity and in doing so forfeited fitness, serum survival, biofilm capacity and decisively carbapenem resistance. Taken together, these results support receptor-informed cocktail design as the appropriate basis for *A. baumannii* phage therapy, and identify phage-driven capsule loss as an evolutionary trade-off that future phage–antibiotic regimens should be designed to exploit. Mammalian pharmacokinetic and efficacy studies are the necessary next step.

Declarations:

Clinical Trial No.

Not applicable

Consent for publication

Not applicable

Availability of data and materials

The dataset used and/or analyzed during the study is available from the corresponding author on request.

Competing interests

The authors declare that they have no competing interests.

Funding

This study did not receive any funding.

Authors' contributions

UF: Conceptualization, Data curation, Formal analysis, Methodology, Writing – original draft. **SAR:** Conceptualization, Methodology, Writing – review & editing. **MJB:** Conceptualization, Methodology, Writing – review & editing.

Acknowledgements

None

References

1. Murray CJL, Ikuta KS, Sharara F, et al. Global burden of bacterial antimicrobial resistance in 2019: a systematic analysis. Lancet. 2022;399(10325):629–655.
2. World Health Organization. WHO bacterial priority pathogens list, 2024: bacterial pathogens of public health importance to guide research, development and strategies to prevent and control antimicrobial resistance. Geneva: WHO; 2024.

Frontier in Medical & Health Research

ISSN: (e) 3007-1607 (p) 3007-1593

3. Wong D, Nielsen TB, Bonomo RA, Pantapalangkoor P, Luna B, Spellberg B. Clinical and pathophysiological overview of Acinetobacter infections: a century of challenges. Clin Microbiol Rev. 2017;30(1):409–447.
4. Nguyen M, Joshi SG. Carbapenem resistance in Acinetobacter baumannii, and their importance in hospital-acquired infections: a scientific review. J Appl Microbiol. 2021;131(6):2715–2738.
5. Hamidian M, Nigro SJ. Emergence, molecular mechanisms and global spread of carbapenem-resistant Acinetobacter baumannii. Microb Genom. 2019;5(10):e000306.
6. Zarrilli R, Pournaras S, Giannouli M, Tsakris A. Global evolution of multidrug-resistant Acinetobacter baumannii clonal lineages. Int J Antimicrob Agents. 2013;41(1):11–19.
7. Tamma PD, Aitken SL, Bonomo RA, Mathers AJ, van Duin D, Clancy CJ. Infectious Diseases Society of America guidance on the treatment of antimicrobial-resistant Gram-negative infections. Clin Infect Dis. 2024;ciae403.
8. Shields RK, Paterson DL, Tamma PD. Navigating available treatment options for carbapenem-resistant Acinetobacter baumannii-calcoaceticus complex infections. Clin Infect Dis. 2023;76(Suppl 2):S179–S193.
9. Schooley RT, Biswas B, Gill JJ, et al. Development and use of personalized bacteriophage-based therapeutic cocktails to treat a patient with a disseminated resistant Acinetobacter baumannii infection. Antimicrob Agents Chemother. 2017;61(10):e00954-17.
10. Dedrick RM, Guerrero-Bustamante CA, Garlena RA, et al. Engineered bacteriophages for treatment of a patient with a disseminated drug-resistant Mycobacterium abscessus. Nat Med. 2019;25(5):730–733.
11. Jault P, Leclerc T, Jennes S, et al. Efficacy and tolerability of a cocktail of bacteriophages to treat burn wounds infected by Pseudomonas aeruginosa (PhagoBurn): a randomised, controlled, double-blind phase 1/2 trial. Lancet Infect Dis. 2019;19(1):35–45.
12. Kortright KE, Chan BK, Koff JL, Turner PE. Phage therapy: a renewed approach to combat antibiotic-resistant bacteria. Cell Host Microbe. 2019;25(2):219–232.
13. Gordillo Altamirano FL, Barr JJ. Phage therapy in the postantibiotic era. Clin Microbiol Rev. 2019;32(2):e00066-18.
14. Oliveira H, Costa AR, Konstantinides N, et al. Ability of phages to infect Acinetobacter calcoaceticus-Acinetobacter baumannii complex species through acquisition of different pectate lyase depolymerase domains. Environ Microbiol. 2017;19(12):5060–5077.
15. Popova AV, Lavysh DG, Klimuk EI, et al. Novel Fri1-like viruses infecting Acinetobacter baumannii — vB_AbaP_AS11 and vB_AbaP_AS12 — characterization, comparative genomic analysis, and host-recognition strategy. Viruses. 2017;9(7):188.
16. Gordillo Altamirano F, Forsyth JH, Patwa R, et al. Bacteriophage-resistant Acinetobacter baumannii are resensitized to antimicrobials. Nat Microbiol. 2021;6(2):157–161.
17. Magiorakos AP, Srinivasan A, Carey RB, et al. Multidrug-resistant, extensively drug-resistant and pandrug-resistant bacteria: an international expert proposal for interim standard definitions for acquired resistance. Clin Microbiol Infect. 2012;18(3):268–281.

Frontier in Medical & Health Research

ISSN: (e) 3007-1607 (p) 3007-1593

18. Wyres KL, Cahill SM, Holt KE, Hall RM, Kenyon JJ. Identification of Acinetobacter baumannii loci for capsular polysaccharide (KL) and lipooligosaccharide outer core (OCL) synthesis in genome assemblies using curated reference databases compatible with Kaptive. Microb Genom. 2020;6(3):e000339.
19. Turner D, Shkoporov AN, Lood C, et al. Abolishment of morphology-based taxa and change to binomial species names: 2022 taxonomy update of the ICTV bacterial viruses subcommittee. Arch Virol. 2023;168(2):74.
20. Wick RR, Judd LM, Gorrie CL, Holt KE. Unicycler: resolving bacterial genome assemblies from short and long sequencing reads. PLoS Comput Biol. 2017;13(6):e1005595.
21. Garneau JR, Depardieu F, Fortier LC, Bikard D, Monot M. PhageTerm: a tool for fast and accurate determination of phage termini and packaging mechanism using next-generation sequencing data. Sci Rep. 2017;7(1):8292.
22. Bouras G, Nepal R, Houtak G, Psaltis AJ, Wormald PJ, Vreugde S. Pharokka: a fast scalable bacteriophage annotation tool. Bioinformatics. 2023;39(1):btac776.
23. Moraru C, Varsani A, Kropinski AM. VIRIDIC — a novel tool to calculate the intergenomic similarities of prokaryote-infecting viruses. Viruses. 2020;12(11):1268.
24. Pirnay JP, Djebara S, Steurs G, et al. Personalized bacteriophage therapy outcomes for 100 consecutive cases: a multicentre, multinational, retrospective observational study. Nat Microbiol. 2024;9(6):1434–1453.
25. Abedon ST, Danis-Wlodarczyk KM, Wozniak DJ. Phage cocktail development for bacteriophage therapy: toward improving spectrum of activity breadth and depth. Pharmaceuticals. 2021;14(10):1019.
26. Chan BK, Abedon ST, Loc-Carrillo C. Phage cocktails and the future of phage therapy. Future Microbiol. 2013;8(6):769–783.
27. Leitner L, Ujmajuridze A, Chanishvili N, et al. Intravesical bacteriophages for treating urinary tract infections in patients undergoing transurethral resection of the prostate: a randomised, placebo-controlled, double-blind clinical trial. Lancet Infect Dis. 2021;21(3):427–436.
28. Hyman P, Abedon ST. Bacteriophage host range and bacterial resistance. Adv Appl Microbiol. 2010;70:217–248.
29. Kutter E. Phage host range and efficiency of plating. Methods Mol Biol. 2009;501:141–149.
30. Knecht LE, Veljkovic M, Fieseler L. Diversity and function of phage encoded depolymerases. Front Microbiol. 2020;10:2949.
31. Pires DP, Oliveira H, Melo LDR, Sillankorva S, Azeredo J. Bacteriophage-encoded depolymerases: their diversity and biotechnological applications. Appl Microbiol Biotechnol. 2016;100(5):2141–2151.
32. Ferriol-González C, Domingo-Calap P. Phages for biofilm removal. Antibiotics. 2020;9(5):268.
33. Chaudhry WN, Concepción-Acevedo J, Park T, Andleeb S, Bull JJ, Levin BR. Synergy and order effects of antibiotics and phages in killing Pseudomonas aeruginosa biofilms. PLoS One. 2017;12(1):e0168615.
34. Tsao YT, Tsai YH, Liao WT, Shen CJ, Shen CF, Cheng CM. Differential markers of bacterial and viral infections in children for point-of-care testing. Trends Mol Med. 2020;26(12):1118–1132.
35. Tacconelli E, Carrara E, Savoldi A, et al. Discovery, research, and development of new antibiotics: the WHO priority list of antibiotic-resistant bacteria and tuberculosis. Lancet Infect Dis. 2018;18(3):318–327.

Frontier in Medical & Health Research

ISSN: (e) 3007-1607 (p) 3007-1593

36. Peleg AY, Seifert H, Paterson DL. Acinetobacter baumannii: emergence of a successful pathogen. Clin Microbiol Rev. 2008;21(3):538–582.
37. Harding CM, Hennon SW, Feldman MF. Uncovering the mechanisms of Acinetobacter baumannii virulence. Nat Rev Microbiol. 2018;16(2):91–102.
38. Geisinger E, Isberg RR. Antibiotic modulation of capsular exopolysaccharide and virulence in Acinetobacter baumannii. PLoS Pathog. 2015;11(2):e1004691.
39. Kenyon JJ, Hall RM. Variation in the complex carbohydrate biosynthesis loci of Acinetobacter baumannii genomes. PLoS One. 2013;8(4):e62160.
40. Timoshina OY, Shneider MM, Evseev PV, et al. Friunavirus phage-encoded depolymerases specific to different capsular types of Acinetobacter baumannii. Int J Mol Sci. 2023;24(11):9100.
41. Liu Y, Leung SSY, Guo Y, et al. The capsule depolymerase Dpo48 rescues Galleria mellonella and mice from Acinetobacter baumannii systemic infections. Front Microbiol. 2019;10:545.
42. Jeon J, Park JH, Yong D. Efficacy of bacteriophage treatment against carbapenem-resistant Acinetobacter baumannii in Galleria mellonella larvae and a mouse model of acute pneumonia. BMC Microbiol. 2019;19(1):70.
43. Tsai CJY, Loh JMS, Proft T. Galleria mellonella infection models for the study of bacterial diseases and for antimicrobial drug testing. Virulence. 2016;7(3):214–229.
44. Pelfrene E, Willebrand E, Cavaleiro Sanches A, Sebris Z, Cavaleri M. Bacteriophage therapy: a regulatory perspective. J Antimicrob Chemother. 2016;71(8):2071–2074.
45. Luong T, Salabarria AC, Roach DR. Phage therapy in the resistance era: where do we stand and where are we going? Clin Ther. 2020;42(9):1659–1680.
46. Nale JY, Clokie MRJ. Preclinical data and safety assessment of phage therapy in humans. Curr Opin Biotechnol. 2021;68:310–317.
47. Hatfull GF, Dedrick RM, Schooley RT. Phage therapy for antibiotic-resistant bacterial infections. Annu Rev Med. 2022;73:197–211.
48. Dąbrowska K, Abedon ST. Pharmacologically aware phage therapy: pharmacodynamic and pharmacokinetic obstacles to phage antibacterial action in animal and human bodies. Microbiol Mol Biol Rev. 2019;83(4):e00012-19.
49. Łusiak-Szelachowska M, Międzybrodzki R, Drulis-Kawa Z, et al. Bacteriophages and antibiotic interactions in clinical practice: what we have learned so far. J Biomed Sci. 2022;29(1):23.
50. Torres-Barceló C, Hochberg ME. Evolutionary rationale for phages as complements of antibiotics. Trends Microbiol. 2016;24(4):249–256.
51. Castledine M, Padfield D, Sierocinski P, et al. Parallel evolution of Pseudomonas aeruginosa phage resistance and virulence loss in response to phage treatment in vivo and in vitro. eLife. 2022;11:e73679.
52. Mangalea MR, Duerkop BA. Fitness trade-offs resulting from bacteriophage resistance potentiate synergistic antibacterial strategies. Infect Immun. 2020;88(7):e00926-19.
53. Egido JE, Costa AR, Aparicio-Maldonado C, Haas PJ, Brouns SJJ. Mechanisms and clinical importance of bacteriophage resistance. FEMS Microbiol Rev. 2022;46(1):fuab048.
54. Dedrick RM, Freeman KG, Nguyen JA, et al. Potent antibody-mediated neutralization limits bacteriophage treatment of a pulmonary Mycobacterium abscessus infection. Nat Med. 2021;27(8):1357–1361.

Frontier in Medical & Health Research

ISSN: (e) 3007-1607 (p) 3007-1593

55. Yehl K, Lemire S, Yang AC, et al. Engineering phage host-range and suppressing bacterial resistance through phage tail fiber mutagenesis. Cell. 2019;179(2):459–469.

56. Hanlon GW. Bacteriophages: an appraisal of their role in the treatment of bacterial infections. Int J Antimicrob Agents. 2007;30(2):118–128.

57. Clinical and Laboratory Standards Institute. Performance standards for antimicrobial susceptibility testing. 33rd ed. CLSI supplement M100. Wayne, PA: CLSI; 2023.

58. European Committee on Antimicrobial Susceptibility Testing. Breakpoint tables for interpretation of MICs and zone diameters. Version 14.0. Växjö: EUCAST; 2024.